IEEE Access
Multidisciplinary ⋮ Rapid Review ⋮ Open Access Journal

Received 6 May 2024, accepted 23 May 2024, date of publication 11 June 2024, date of current version 18 June 2024.

Digital Object Identifier 10.1109/ACCESS.2024.3412404

RESEARCH ARTICLE

Comparative Analysis of Inner and Outer Rotor Surface PM Machines Based on Optimization Dataset

DONG MYEONG CHOI, (Student Member, IEEE), AND SEUN GUY MIN, (Member, IEEE)
Department of Electrical Engineering, Soongsil University, Seoul 06978, South Korea
Corresponding author: Seun Guy Min (sgmin19@ssu.ac.kr)

ABSTRACT This paper examines and compares the performance characteristics of inner and outer rotor surface permanent magnet (SPM) machines. Notably, this research distinguishes itself through a rigorous methodology that carefully selects an optimization dataset rather than relying on arbitrary data. Consequently, this methodology has yielded valuable insights in two significant aspects: 1) The trends of key design parameters for both inner and outer rotor types, such as split ratio, aspect ratio, and magnet-gap ratio, are revealed using the optimization dataset. 2) The torque-to-weight ratio values between the inner and outer rotor types are investigated from various perspectives. Through this analysis, it becomes numerically evident that a significant advantage can be obtained using the outer rotor type compared to the inner rotor type. Overall, this study provides valuable insights for researchers, particularly those involved in the initial design stage of SPM machines for both rotor types.

INDEX TERMS Analytical model, differential evolution, inner rotor, optimization, outer rotor, surface permanent magnet motor, torque density.

I. INTRODUCTION

In recent years, advancements in production and application technologies have led to the development of permanent magnet (PM) machines, which provide high torque density, high efficiency, and accurate position/speed control [1], [2], [3]. As a result of these advantages, PM machines are now widely used in various applications, such as aerospace, industrial automation, electric vehicles, and wind power generators [4], [5], [6]. Based on the location of the rotor magnets, PM machines can be classified into two types: inner rotor and outer rotor. Thus, conducting a comprehensive performance evaluation and comparing these two types can provide valuable insights, especially during the initial phases of motor design.

Obtaining optimized geometric data is crucial to ensure a fair comparison. In particular, weight optimization stands out as a more impartial approach than loss and cost optimization. While loss optimization focuses mainly on reducing copper weight, and cost optimization targets magnet weight reduction, these methods prove inadequate due to their narrow scope. Conversely, weight optimization offers a balanced reduction in the weight of iron, copper, and magnets. Therefore, the design parameters derived from weight optimization serve as invaluable references during the initial design phases.

To our knowledge, previous research comparing the inner and outer rotor types can be found as follows: The motor constant and nominal torque for both inner and outer rotor types were optimized as discussed in [7]. This optimization utilized a single-objective genetic algorithm. However, it focused solely on incrementally adjusting the inner or outer radius and active length, with the remaining design parameters constant. In [8], two motor types for e-bikes were discussed, with an inner rotor type being recommended due to its lower loss and weight compared to an outer rotor type. In [9], the performance of inner and outer rotor types was compared by changing magnet arrangement,

The associate editor coordinating the review of this manuscript and approving it for publication was R. K. Saket.

number of poles, and current density. Additionally, a comparison of the design performances between inner and outer rotor permanent magnet alternators, analyzed through finite elements, was conducted in [10]. However, these studies conducted comparative analyses on arbitrarily chosen sample data, needing a comprehensive comparative analysis with optimized data. This is a recurring issue identified in past published works, where such approaches cannot yield fair and objective research results. Meanwhile, the optimal split ratio was determined in [11] to evaluate the torque density between the inner and outer rotor configurations. In [12], a comparison of inner and outer rotor AFPM machines was discussed in terms of torque quality. Despite attempts to incorporate the optimization results from [11] and [12], these studies still have limitations due to their reliance on a fundamental sizing equation instead of a large-scale design optimization methodology.

More recently, Wu et al. [13] investigated the unbalanced magnetic force of asymmetric PM machines, considering both inner and outer rotor topologies. Barranco et al. [14] analyzed heat transfer in the end-space region of fractional-slot concentrated windings, observing divergent trends in thermal coefficients for inner and outer rotor designs. Deng et al. [15] investigated the effect of eccentricity on the electromagnetic force and unbalanced bending moment in inner and outer rotor configurations. Shi and Ching [16] presented a method to maximize the power factor while considering the allocation of turn-number for the inner and outer stator windings. However, the design parameters were not optimized in these studies. They obtained a dataset utilizing arbitrary geometric parameters. Jung et al. [17] conducted a design comparison between the inner and outer rotor HTS machines based on multi-objective optimization.

Although earlier publications [7], [8], [9], [10], [11], [12], [13], [14], [15], [16], [17] have provided specific insights, the key research gaps about this topic can be summarized in the following manners:

1) Prior research predominantly did not employ optimized data when evaluating the performance characteristics of inner and outer rotor configurations. The sole exception is [17], where multi-objective optimization was carried out using NSGA-III for the design comparison. Nevertheless, this manuscript focused on high-speed applications, and no examination was carried out from the viewpoint of low-speed/high torque.
2) To date, no previous research has compared the optimal values of design parameters for inner and outer rotor configurations. Such a study would serve as valuable reference material in the initial design phase of PM machines.
3) It is widely acknowledged that the outer rotor type exhibits higher torque density than the inner rotor type under identical conditions and dimensions [11]. Nevertheless, it is challenging to discover research works that comprehensively investigate the underlying reasons and quantify their degree numerically through detailed design analysis.

To address these research gaps, this paper examines and contrasts the performance characteristics of inner and outer rotor PM machines utilizing optimal design solutions selected from a pool of numerous candidates. To attain precise and expeditious optimal solutions, the analytical model based on the complex permeance (CP) function [18] is integrated with the differential evolution (DE) algorithm. In this study, the performance comparison is mainly executed from an active weight perspective. The rationale behind this choice is that active weight is the metric that represents the overall performance more effectively than any other factors [19], [20]. Consequently, this research has yielded valuable insights into four significant aspects:

1) The analytical model applicable to both inner and outer rotor types is developed, revealing that a separate calculation of flux density for both rotor types is unnecessary.
2) The optimization dataset shows the trends of key design parameters for both types, such as split ratio, aspect ratio, and magnet-gap ratio.
3) The analysis of the torque-to-weight ratio for the inner and outer rotor configurations demonstrates numerically the extent of the advantage afforded by using the outer rotor type.
4) The performance trends of the inner and outer rotor types with respect to changes in design parameters are shown.

These insights will be helpful not only for the academic understanding of inner and outer rotor types but also in the design phase. The research results are more accurate and reasonable because they are based on optimization data.

The following sections of this paper are structured as follows: Section II proves that the residual flux density for inner and outer rotor types is identical and presents an analytical model applicable to both types. Section III validates the proposed analytical model through comparison with finite element (FE) and experimental results. Section IV conducts a comprehensive design optimization utilizing the DE algorithm and compares inner and outer rotor types based on acquired optimization data. Finally, Section V summarizes this work.

II. ANALYTICAL MODEL

This section presents an analytical model using the CP model, applicable to both inner and outer rotor configurations. Fig. 1 shows cross-sectional depictions of both rotor types. As illustrated in Fig. 1, the machine topology under consideration in this study is surface-mounted PM (SPM) machines.

A. OPEN-CIRCUIT MAGNETIC FIELD IN SLOTLESS AIR GAP

Calculating the open-circuit magnetic field is an essential task that must be given priority. This computation, presented

in [21], has been cited and utilized in numerous scholarly publications. As stated in [21], separate field equations were derived for inner and outer rotor types, with the relevant formulas expressed in (1) and (2), as shown at the bottom of the page, and have been used independently until now. In (1) and (2), B_r is the residual flux density, μ_0 is the permeability of free space, μ_r is the relative permeability of magnet, M is the residual magnetization, p is the number of pole pairs, r is target radius, and A_{3n} is given by

$$A_{3n} = \begin{cases} 2\dfrac{M_{r1}}{M_1} - 1 & \text{for } np{=}1 \quad (3) \\ \left(np - \dfrac{1}{np}\right)\dfrac{M_{rn}}{M_n} + \dfrac{1}{np} & \text{for } np \neq 1 \quad (4) \end{cases}$$

where M_r is radial magnetization, R_r is the radius of the rotor yoke, R_m is the radius of the magnet surface, and R_s is the radius of the stator bore.

Equations (1) and (2) illustrate the radial flux density in the air gap for each rotor type. Fig. 2 represents (1) and (2) graphically for better understanding. As indicated in (1) and (2), the derived formulas for the inner and outer types appear dissimilar, and as such, these two formulas have been employed independently up to this point. However, it will be demonstrated that these two seemingly different formulas are, in fact, identical.

Through the utilization of symbols defined in bold red color within (1) and (2), formulas can be simplified and expressed as follows:

***For inner rotor type*:**

$$B_r(r,\theta) = \sum_{n=1,3,5,\ldots} \beta_1\beta_2\beta_3 \cos(np\theta) \quad (5)$$

***For outer rotor type*:**

$$B_r(r,\theta) = \sum_{n=1,3,5,\ldots} -\beta_1\beta_4\beta_5 \cos(np\theta) \quad (6)$$

The four variables β_2, β_3, β_4, and β_5 are related as follows:

$$\beta_2 = \beta_4 \left(\frac{R_m}{R_s}\right)^{2np} \quad (7)$$

$$\beta_3 = \beta_5 \frac{(R_r/R_m)^{2np}}{-(R_r/R_s)^{2np}} = -\beta_5 \left(\frac{R_s}{R_m}\right)^{2np} \quad (8)$$

Substituting (7) and (8) into (5) yields

$$\begin{aligned} &B_r(r,\theta) \\ &= \sum_{n=1,3,5,\ldots} -\beta_1\beta_4\beta_5 \left(\frac{R_m}{R_s}\right)^{2np}\left(\frac{R_s}{R_m}\right)^{2np} \cos(np\theta) \\ &= \sum_{n=1,3,5,\ldots} -\beta_1\beta_4\beta_5 \cos(np\theta) \end{aligned} \quad (9)$$

As demonstrated in (9), despite the initial appearance of substantial divergence in the formulations for the inner and outer rotor types, it becomes manifest that both equations are essentially equivalent. Consequently, many academic publications have divided the same formula into inner and outer types and utilized them separately. Although this discovery may not have significant practical implications, it holds

***For inner rotor type*:**

$$B_r(r,\theta) = \sum_{n=1,3,5,\ldots,} \underbrace{\frac{\mu_0 M_n}{\mu_r}\frac{np}{(np)^2-1}}_{\beta_1} \underbrace{\left(\left(\frac{r}{R_s}\right)^{np-1}\left(\frac{R_m}{R_s}\right)^{np+1} + \left(\frac{R_m}{r}\right)^{np+1}\right)}_{\beta_2} \cdot \underbrace{\left\{\frac{(A_{3n}-1) + 2\left(\frac{R_r}{R_m}\right)^{np+1} - (A_{3n}+1)\left(\frac{R_r}{R_m}\right)^{2np}}{\frac{\mu_r+1}{\mu_r}\left[1-\left(\frac{R_r}{R_s}\right)^{2np}\right] - \frac{\mu_r-1}{\mu_r}\left[\left(\frac{R_m}{R_s}\right)^{2np} - \left(\frac{R_r}{R_m}\right)^{2np}\right]}\right\}}_{\beta_3} \cos(np\theta) \quad (1)$$

***For outer rotor type*:**

$$B_r(r,\theta) = \sum_{n=1,3,5,\ldots} \underbrace{-\frac{\mu_0 M_n}{\mu_r}\frac{np}{(np)^2-1}}_{\beta_1} \cdot \underbrace{\left(\left(\frac{r}{R_m}\right)^{np-1} + \left(\frac{R_s}{R_m}\right)^{np-1}\left(\frac{R_s}{r}\right)^{np+1}\right)}_{\beta_4} \cdot \underbrace{\left\{\frac{(A_{3n}-1)\left(\frac{R_m}{R_r}\right)^{2np} + 2\left(\frac{R_m}{R_r}\right)^{np-1} - (A_{3n}+1)}{\frac{\mu_r+1}{\mu_r}\left[1-\left(\frac{R_s}{R_r}\right)^{2np}\right] - \frac{\mu_r-1}{\mu_r}\left[\left(\frac{R_s}{R_m}\right)^{2np} - \left(\frac{R_m}{R_r}\right)^{2np}\right]}\right\}}_{\beta_5} \cos(np\theta) \quad (2)$$

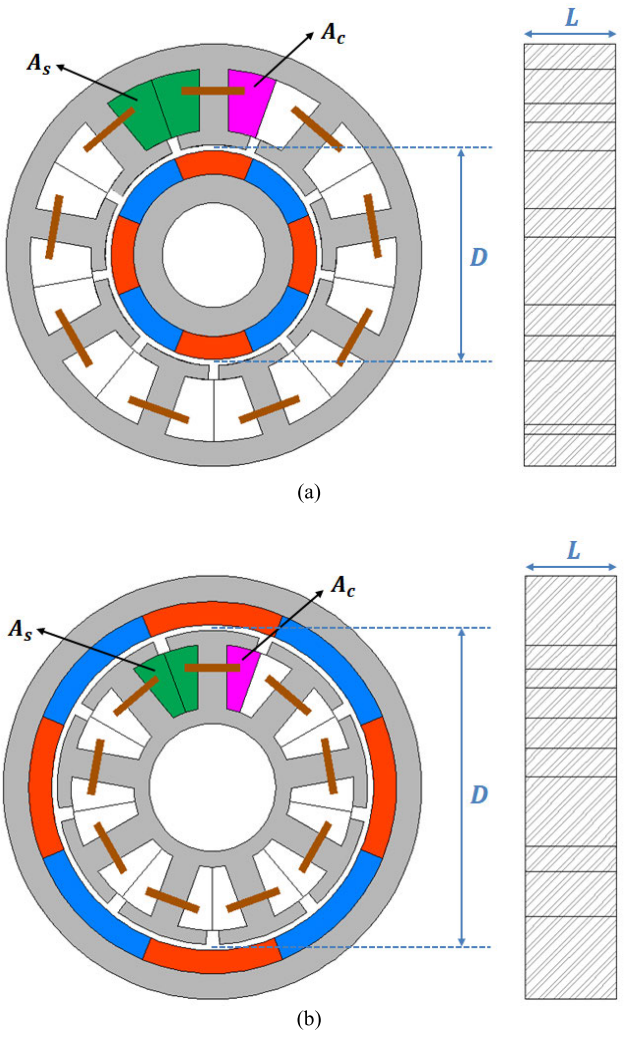

FIGURE 1. 2-D cross-sectional depiction of SPM machines with (a) inner rotor type (b) outer rotor type.

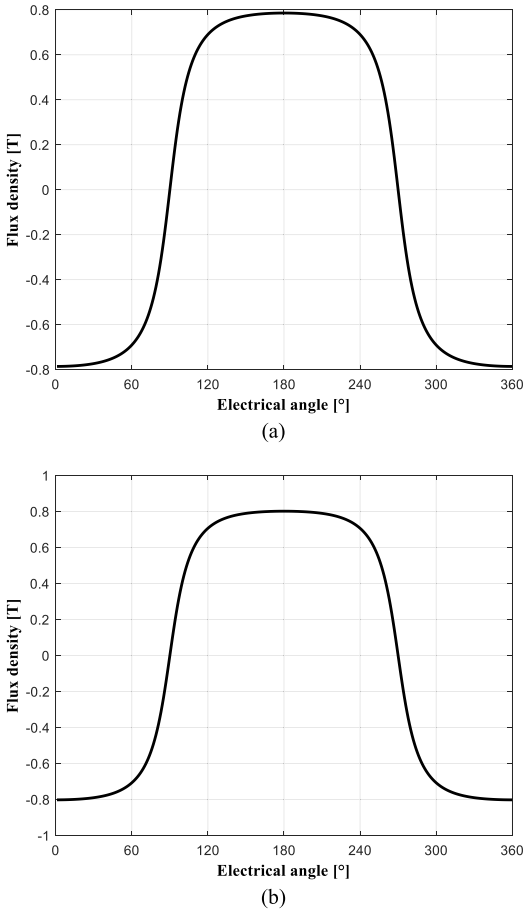

FIGURE 2. Radial flux density of SPM machines for (a) inner rotor type (b) outer rotor type.

undeniable academic significance. Besides, consolidating two equations into one can simplify the analytical model, resulting in reduced computational time for the optimization of both inner and outer rotor configurations. As with the radial flux density, distinct formulas were derived for the tangential flux density of inner and outer types [21]. However, both essentially represent the same formula following the principle explained earlier. Therefore, in this paper, the calculation of the magnetic flux density will be unified instead of being distinguished between inner and outer rotor configurations.

B. ELECTROMAGNETIC TORQUE

As stated in Section I, the CP model, initially proposed by Zarko et al. [18], is employed in this paper to account for the slotting effects. This model facilitates an explicit formulation of the electromagnetic torque in the following expressions [22]:

$$\begin{aligned} T_{em}(\Theta) &= \sum_{\substack{n=6k\pm1 \\ h=0,1,2,\ldots}} \frac{3\sqrt{2}}{2} DLn_c A_c f_f J_{cu} k_{dn} k_{on} \Big[B_{rn}\lambda_o k_{pn} \\ &\quad + \sum_j \frac{np\left(B_{rn}\lambda_{aj} - B_{\theta n}\lambda_{bj}\right)}{2\left(np + jQ_s\right)} \sin\left(\frac{(np+jQ_s)}{2}\tau_c\right) \\ &\quad + \sum_j \frac{np\left(B_{rn}\lambda_{aj} + B_{\theta n}\lambda_{bj}\right)}{2\left(np - jQ_s\right)} \sin\left(\frac{(np-jQ_s)}{2}\tau_c\right)\Big] \\ &\quad \cdot \cos(6hp\Theta) \end{aligned} \tag{10}$$

where D is the air gap diameter, L is the active length, n_c is the number of coils per phase, A_c is the cross-sectional coil area, f_f is the fill factor, J_{cu} is the root mean square value of current density, k_{dn} is the distribution factor, k_{on} is the slot opening factor, k_{pn} is the pitch factor, and B_{rn} and $B_{\theta n}$ are the radial and tangential components of the flux density in the slotless air gap, λ_o is the mean value of the CP function, λ_{aj} and λ_{bj} are harmonics of real and imaginary components of the CP

function, respectively, Q_s is the number of slots, and τ_c is the coil pitch.

Based on (10), the average value of electromagnetic torque can be obtained as

$$T_{avg} = \frac{3\sqrt{2}}{2} D L n_c A_c f_f J_{cu} B_{r1} k_{w1} \lambda_o \tag{11}$$

where k_{w1} denotes the fundamental component of comprehensive winding factor, which can be expressed as $k_{w1} = k_{p1} k_{d1} k_{o1}$.

In order to depict the aforementioned equation in a more refined manner, the variables A_c and n_c are represented as:

$$\begin{cases} A_c = \dfrac{A_{slot}}{\eta} \\ n_c = \dfrac{Q_s \eta}{6} \end{cases} \tag{12}$$

where A_{slot} is the cross-sectional slot area and η is the number of slot layers. For example, the value of η is 2 in the configuration shown in Fig. 1.

By substituting (12) into (11), the average torque can be refined as follows:

$$\begin{aligned} T_{avg} &= \frac{\sqrt{2}}{4} D L Q_s A_{slot} f_f J_{cu} B_{r1} k_{w1} \lambda_o \\ &= \frac{\sqrt{2}}{4} D L \boldsymbol{\xi_e} f_f J_{cu} B_{r1} k_{w1} \lambda_o \end{aligned} \tag{13}$$

where the symbol ξ_e represents the electrical loading surface, which is defined as the total cross-sectional area of slots and can be computed using the expression $\xi_e = Q_s A_{slot}$.

To facilitate an unbiased comparison between the inner and outer rotor types, it is assumed that the motor frame size, pole/slot combination, manufacturing environment, and heat dissipation conditions are all maintained as identical. Given this premise, the design variables L, f_f, J_{cu}, B_{r1}, k_{w1}, and λ_o can be applied with consistent values to both types (Owing to the variation in the width dimensions of the magnet, the value of B_{r1} is not completely identical. However, considering the projected differences are expected to be insignificant, it is posited that B_{r1} remains uniform for the current period).

Consequently, the design variables that cause differences in the torque formula between the inner and outer rotor types will be the air gap diameter and electrical loading, which are indicated in bold blue in (13).

As illustrated in Fig. 1, it is evident that the air gap diameter in the outer rotor type exceeds that of the inner rotor type. This is due to the stator slot of the outer rotor type being situated internally, thereby forcing the air gap to extend further outward than in the inner rotor type under equivalent outer diameter conditions. Thus, from the viewpoint of the air gap diameter, it can be inferred that the outer rotor type, possessing greater rotational inertia, offers superior torque advantages over the inner rotor type.

Conversely, as depicted in Fig. 1, the electrical loading surface is greater in the inner rotor type compared to the outer rotor type. This dissimilarity is attributed to the fact that the inner rotor type, with the stator slot positioned on the circle's exterior, is bound to have a larger total cross-sectional slot area than the outer rotor type, given the same geometric conditions. The expressions for the electrical loading surface for each rotor type can be formulated as follows:

***For inner rotor type*:**

$$\xi_e = \frac{\pi \left((D + 2h_{s0} + 2h_{s2})^2 - (D + 2h_{s0})^2 \right)}{4} - T_w h_{s2} Q_s \tag{14}$$

***For outer rotor type*:**

$$\xi_e = \frac{\pi \left((D - 2h_{s0})^2 - (D - 2h_{s0} - 2h_{s2})^2 \right)}{4} - T_w h_{s2} Q_s \tag{15}$$

where h_{s0} is the slot opening height, h_{s2} is the slot height, and T_w is the stator tooth width.

The required stator tooth width to avoid iron saturation can be determined as follows:

$$T_w = \frac{\pi D}{Q_s} \times \frac{B_{g\_max}}{B_{fe\_max}} \tag{16}$$

where B_{fe_max} is the maximum allowable flux density of the ferromagnetic material and B_{g_max} is the maximum flux density in the air gap traveling through the tooth winding.

Assuming the neglect of the armature reaction field, B_{g_max} can be achieved when the center of the magnet coincides with the center of the tooth width, calculated as follows:

$$B_{g\_max} = \frac{Q_s}{2\pi} \int_{-\frac{\pi}{Q_s}}^{\frac{\pi}{Q_s}} B_{r1} \cos p\theta d\theta = \frac{B_{r1} Q_s}{\pi p} \sin\left(\frac{\pi p}{Q_s}\right) \tag{17}$$

Overall, the air gap diameter is expected to be greater in the outer rotor type than in the inner rotor type. In contrast, the electrical loading surface is anticipated to yield the opposite result. Ultimately, these two design variables (D and ξ_e) can be viewed as forming a trade-off relationship regarding torque production. Therefore, a comparison of torque production between the inner and outer rotor types depends on which variable exerts a more substantial impact. As stated in Section I, an equitable comparison necessitates the utilization of optimized data instead of arbitrarily selected sample data, which will be extensively elaborated upon in Section IV.

C. ACTIVE WEIGHT

As presented in Section I, this study mainly undertakes a performance comparison of the inner and outer rotor configurations from the perspective of active weight. This approach has been adopted since active weight, as a solitary metric, provides a comprehensive assessment of the overall performance of PM machines without bias towards one particular indicator. Consequently, if the active weight is optimized, it can be postulated that other performances, such as loss or material cost, are also optimized to a certain extent.

The active weight can be segregated into four constituent parts, namely, PMs, stator core, rotor core, and copper winding. The weight of each component for both rotor types can be determined using the following expressions:

***For inner rotor type*:**

$$\varpi_{PM} = \frac{\pi}{4}\left(D^2 - (D-2h_m)^2\right)\alpha_p L\delta_{PM} \tag{18}$$

$$\varpi_{rc} = \frac{\pi}{4}\left((D-2h_m)^2 - (D-2h_m-2\Upsilon_{BI})^2\right)L\delta_{fe} \tag{19}$$

$$\begin{aligned}\varpi_{sc} &= \underbrace{\frac{\pi}{4}\left((D+2h_s+2\Upsilon_B)^2-(D+2h_s)^2\right)L\delta_{fe}}_{Backiron} \\ &+ \underbrace{\frac{\pi}{4}\left((D+2h_{s0})^2-D^2\right)(1-\beta_{s0})L\delta_{fe}}_{Tip} \\ &+ \underbrace{Q_s h_{s2} T_w L\delta_{fe}}_{Tooth}\end{aligned} \tag{20}$$

$$\begin{aligned}\varpi_{cu} &\coloneqq \underbrace{\xi_e f_f (2L)\delta_{cu}}_{Active} \\ &+ \underbrace{\xi_e f_f \frac{2\pi\,(D+2h_{s0}+h_{s2})}{Q_s}\delta_{cu}}_{End\ winding}\end{aligned} \tag{21}$$

***For outer rotor type*:**

$$\varpi_{PM} = \frac{\pi}{4}\left((D+2h_m)^2 - D^2\right)\alpha_p L\delta_{PM} \tag{22}$$

$$\varpi_{rc} = \frac{\pi}{4}\left((D+2h_m+2\Upsilon_{BI})^2 - (D+2h_m)^2\right)L\delta_{fe} \tag{23}$$

$$\begin{aligned}\varpi_{sc} &= \underbrace{\frac{\pi}{4}\left((D-2h_s)^2-(D-2h_s-2\Upsilon_{BI})^2\right)L\delta_{fe}}_{Backiron} \\ &+ \underbrace{\frac{\pi}{4}\left(D^2-(D-2h_{s0})^2\right)(1-\beta_{s0})L\delta_{fe}}_{Tip} \\ &+ \underbrace{Q_s h_{s2} T_w L\delta_{fe}}_{Tooth}\end{aligned} \tag{24}$$

$$\begin{aligned}\varpi_{cu} &\coloneqq \underbrace{\xi_e f_f (2L)\delta_{cu}}_{Active} \\ &+ \underbrace{\xi_e f_f \frac{2\pi\,(D-2h_{s0}-h_{s2})}{Q_s}\delta_{cu}}_{End\ winding}\end{aligned} \tag{25}$$

where h_m is the magnet thickness, α_p is the pole-arc to pole-pitch ratio, δ_{PM}, δ_{fe}, and δ_{cu} are the density of the magnet, ferromagnetic iron, and copper winding, respectively, Υ_{BI} is the back iron thickness (i.e., $\Upsilon_{BI} = T_w/2$), h_s is the summation of h_{s0} and h_{s2} (i.e., $h_s = h_{s0} + h_{s2}$), and β_{s0} is the slot opening to slot pitch ratio.

D. LOSS AND COST

Along with the primary metric, active weight, the secondary metrics of loss and cost are also considered in the comparative analysis between inner and outer rotor types. As this study centers on the operation featuring low-speed and high torque, the Joule loss is exclusively incorporated in the loss calculation, which can be formulated using the following equation:

$$\begin{aligned}P_{cu} &= 3\left(\frac{A_c f_f J_{cu}}{N_c}\right)^2\left(\rho_{cu}\frac{n_c N_c\,(2L+2l_e)}{A_c f_f/N_c}\right) \\ &= 6\boldsymbol{A_c} f_f J_{cu}^2 \rho_{cu} n_c\,(L+l_e)\end{aligned} \tag{26}$$

where ρ_{cu} is the resistivity of the copper material and l_e is the average length of the end coil on a single side of the machine.

The material costs associated with PM machines can be estimated by employing the subsequent standards: PMs (U.S. \$125/kg), copper winding (U.S. \$10/kg), and iron (U.S. \$2.5/kg), as established by

$$C_\chi = \mathbf{125}\boldsymbol{\varpi_{PM}} + 2.5\,(\varpi_{sc}+\varpi_{rc}) + 10\varpi_{cu} \tag{27}$$

As shown in (27), magnets represent the predominant proportion of the material cost for PM machines. Hence, it can be asserted that the material cost is determined by the quantity of magnets utilized.

Overall, the copper loss is determined by the amount of coil used (i.e., electrical loading surface), whereas the material cost can be attributed to the quantity of magnet used. As such, copper loss and material cost exhibit a bias towards specific components, making them unsuitable as primary metrics to signify the comprehensive performance of PM machines.

In Section IV, a performance analysis will be carried out using a multi-objective optimization approach, wherein loss and cost will be aligned with active weight. This will enable a comparative assessment of the inner and outer rotor configurations.

III. FE AND EXPERIMENTAL VALIDATIONS

This paper has utilized an optimization dataset to conduct a comprehensive performance analysis between the inner and outer rotor types. However, this optimization dataset has been generated using the analytical model presented in Section II to achieve expeditious optimal solutions. As a result, it is necessary to validate the accuracy of the analytical model employed within this study. This section centers on verifying the analytical model introduced in Section II through FE and experimental results.

To verify the reliability of the analytical model, the prototype machines were fabricated for both inner and outer rotor configurations. The relevant photographs are depicted in Fig. 3. The major design parameters of these prototype machines are listed in Table 1.

Fig. 4 presents a torque-current characteristic comparison involving analytical, FE, and experimental results. The analytical results align remarkably well with both the FE and experimental results. Consequently, the reliability of the

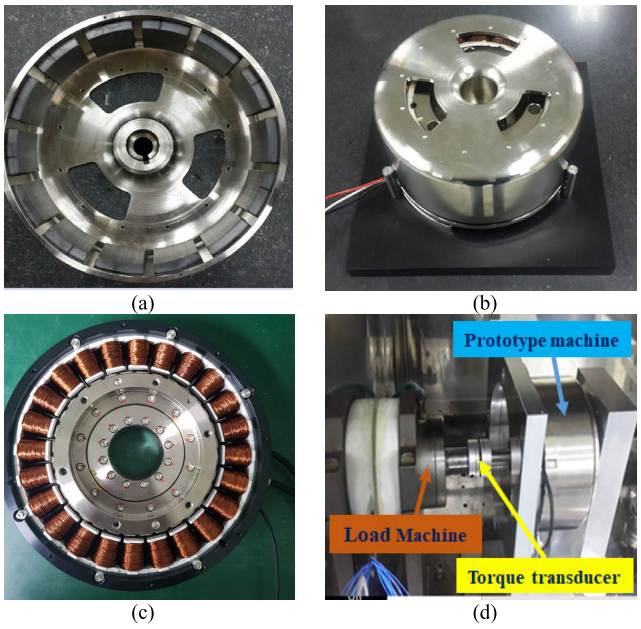

FIGURE 3. Configuration of fabricated PM machines and its corresponding test bench. (a) Rotor magnet assembly for outer rotor type. (b) Entire assembly for outer rotor type. (c) Entire assembly for inner rotor type. (d) Dynamo test setup.

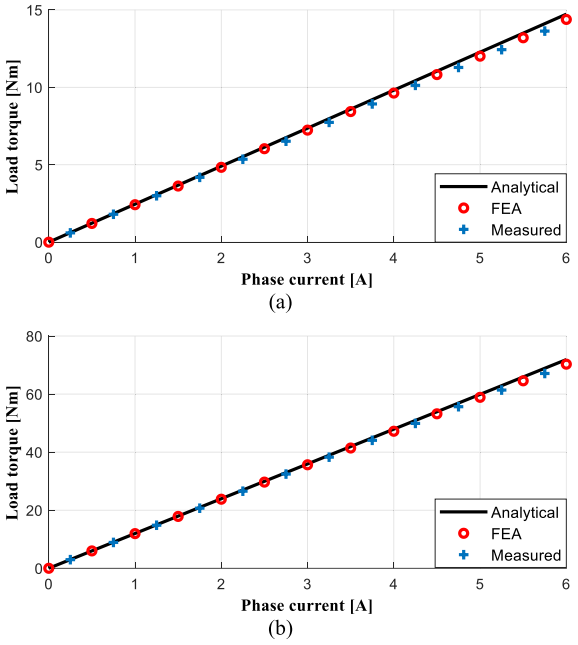

FIGURE 4. Comparison of torque-current characteristics for (a) outer rotor type model (b) inner rotor type.

analytical approach used to gather optimization data has been robustly confirmed.

IV. DESIGN OPTIMIZATION

This section conducts design optimization and establishes a performance comparison between the inner and outer rotor types using the acquired optimization data. Given the complexity of non-linear motor problems, meta-heuristic algorithms can effectively address such optimization challenges. In this section, the optimization problem is resolved by the adoption of the DE algorithm [23], recognized as a pragmatic approach to attaining global optimization. Consequently, this section presents the trends in key design parameters extracted from the optimization dataset, thereby offering a comprehensive performance comparison between the two rotor types.

TABLE 1. Major design parameters of manufactured prototype machine.

Parameter	Unit	Outer	Inner
Number of poles	-	14	32
Number of slots	-	18	24
Air gap diameter	mm	166	151
Outer diameter	mm	190	222
Active length	mm	50.6	35
Air gap	mm	1	1.4
Fill factor	-	0.44	0.42
Magnet thickness	mm	8	5
Pole arc ratio	-	0.9	0.8
Slot height	mm	26.4	26.6
Residual flux density	T	0.44	1.305
Tooth width	mm	6.6	8
Slot opening factor	-	0.25	0.5

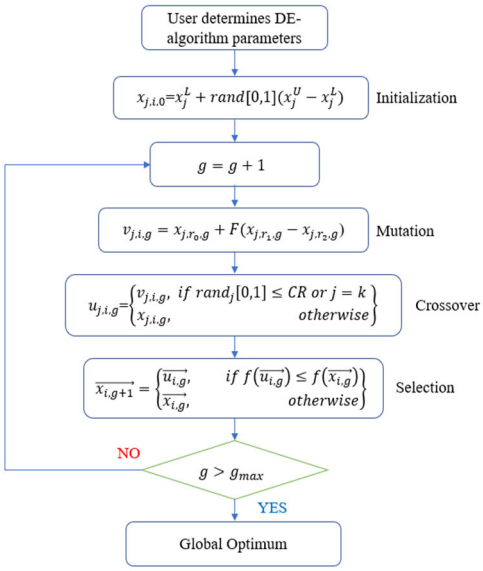

FIGURE 5. Flowchart of DE algorithm.

A. DIFFERENTIAL EVOLUTION ALGORITHM

Fig. 5 illustrates the flowchart of the DE algorithm, a method pioneered by Storn and Price [23], consisting of four main phases: initialization, mutation, crossover, and selection. The DE algorithm allows users to specify various control parameters, such as the dimension of the vector, population size, maximum number of generations, crossover ratio, and mutation factor. Table 2 shows the algorithm parameters employed in this study.

TABLE 2. De algorithm parameters.

Parameter	Symbol	Value
Dimension of vector	D	4
Population size	N	40
Maximum number of generations	g_{max}	200
Crossover ratio	CR	0.3
Mutation factor	F	0.5

TABLE 3. Computational times for meta-heuristic algorithms.

Population size	Algorithms	Number of iterations	Objective function	Time [s]
$N = 10$	DE	25	1.7339	1.06
	GWO	78	1.7347	28.30
	SCA	92	1.7353	1.92
	PSO	16	1.7349	1.68
	TLBO	26	1.7348	1.70
$N = 30$	DE	22	1.7345	2.68
	GWO	75	1.7341	435.08
	SCA	92	1.7347	5.75
	PSO	14	1.7341	3.60
	TLBO	26	1.7338	4.90

B. OBJECTIVE FUNCTION AND DESIGN PARAMETERS

This paper incorporates three components into the objective function: weight, loss, and cost. The formulation of the objective function can be expressed as follows:

$$f_{obj} = C_1 W + C_2 \frac{P_{cu}}{30} + C_3 \frac{C_\chi}{15} + f_{pen} \tag{28}$$

where W is the total weight (i.e., $W = \varpi_{PM} + \varpi_{rc} + \varpi_{sc} + \varpi_{cu}$), P_{cu} is the loss, C_1 is the weighting factor of the total weight, C_2 is the weighting factor of the loss, C_3 is the weighting factor of the material costs, and f_{pen} is the penalty function to avoid unwanted values, such as parameters being negative.

The coefficients 30 for $C_2 P_{cu}$ and 15 for $C_3 C_\chi$ have been applied to achieve equilibrium between their respective values. The penalty function is formulated to comply with the following criterion:

$$f_{pen}^1 : D > 0 \tag{29}$$
$$f_{pen}^2 : h_m > 0 \tag{30}$$
$$f_{pen}^3 : h_{s2} > 0 \tag{31}$$
$$f_{pen}^4 : 0 < \alpha_p < 1 \tag{32}$$
$$f_{pen}^5 : pf > 0.9 \tag{33}$$

The workflow of the proposed optimization model is depicted in Fig. 6, detailing the data optimization process. This workflow demonstrates how optimization data is derived through a specific procedure. Initially, the DE algorithm is applied to four optimization variables: air gap diameter, magnet thickness, pole arc ratio, and slot height. These optimization variables, along with the fixed parameters listed in Table 4, determine the remaining motor variables. Finally, the desired data is extracted by fine-tuning the weighting factors (i.e., $\boldsymbol{C_1}$, $\boldsymbol{C_2}$, and $\boldsymbol{C_3}$) of the objective function.

TABLE 4. Fixed parameters.

Parameter	Symbol	Unit	Value
Air gap	g	mm	1
Fill factor	f_f	-	0.5
Current density	J_{rms}	A_{rms}/mm^2	5
Residual flux density	B_r	T	1.035
Saturation flux density	B_{sat}	T	1.6
Number of poles	p	-	20
Number of slots	Q_s	-	18
Slot opening height	h_{s0}	mm	2
Slot opening factor	b_{s0}^{factor}	-	0.2

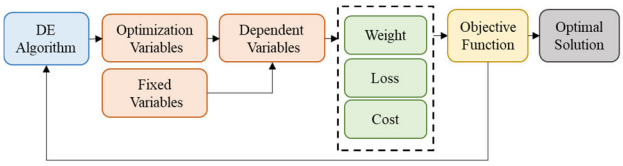

FIGURE 6. Workflow of the proposed optimization method.

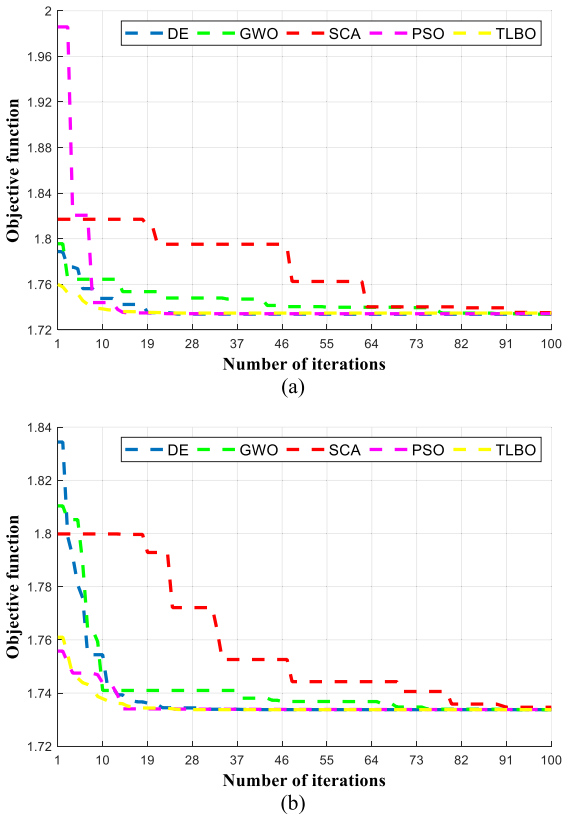

FIGURE 7. Comparison objective function of five different meta-heuristic algorithms at $g_{max} = 100$. (a) $N = 10$. (b) $N = 30$.

C. COMPARISON OF COMPUTATIONAL TIMES FOR META-HEURISTIC ALGORITHMS

This section presents a comparative analysis of five meta-heuristic algorithms: differential evolution (DE), grey wolf optimizer (GWO), sine cosine algorithm (SCA), particle swarm optimization (PSO), and teaching-learning-based optimization (TLBO). Fig. 7 illustrates the objective function

TABLE 5. Target design.

Parameter	Symbol	Unit	Value
Maximum speed	w_{max}	rpm	500
Maximum voltage	V_{max}	V	170

TABLE 6. Design parameters of inner rotor type optimized for minimal active weight.

Torque [Nm]	D [mm]	h_m [mm]	α_p	h_{s2} [mm]	ξ_e [mm^2]
1	78.9435	3.0197	0.7503	8.7855	1951.32
2	90.8548	3.3205	0.7270	10.6163	2691.16
4	105.0747	3.6453	0.7068	12.7910	3729.33
8	122.0015	3.9912	0.6896	15.3797	5195.74
12	133.3480	4.2018	0.6809	17.1184	6296.66
15	140.9640	4.4209	0.6761	17.9751	6990.21
20	148.1720	4.9509	0.6795	18.9836	7434.71

TABLE 7. Design parameters of outer rotor type optimized for minimal active weight.

Torque [Nm]	D [mm]	h_m [mm]	α_p	h_{s2} [mm]	ξ_e [mm^2]
1	92.0199	3.0831	0.6400	15.0797	2198.01
2	106.1638	3.3563	0.6223	17.9444	3037.48
4	122.9415	3.6419	0.6074	21.3553	4198.65
8	143.3773	4.0144	0.5958	25.0642	5763.02
12	159.5172	4.5883	0.5913	25.5967	6497.78
15	168.5799	4.9950	0.5911	26.3480	7459.23
20	180.0182	5.5431	0.5847	26.9548	7605.56

of these five algorithms, aiding in determining the convergence iterations for $N = 10$ and $N = 30$, with a maximum iteration limit of 100. The computational times for these metaheuristic algorithms are provided in Table 3. Table 3 demonstrates that the DE algorithm exhibits the fastest computational time, indicating its superior suitability for this analytical model.

D. PERFORMANCE ANALYSIS OF INNER AND OUTER ROTOR TYPES

Table 4 displays the fixed parameters, while Table 5 presents the target designs. As discussed, this study primarily focuses on comparing performance from the perspective of active weight, as it serves as a more effective metric for overall performance compared to other factors [20]. Accordingly, in this scenario, the weighting factors C_2 and C_3 are assigned zero value. Table 6 presents the optimized design parameters for the inner rotor type, focused on minimizing active weight, while Table 7 summarizes those for the outer rotor type, aimed at achieving the same goal.

In Section II, it was initially expected that the air gap diameter of the outer rotor type would exceed that of the inner rotor type, along with the anticipation that the electrical loading surface of the inner rotor type would be larger than that of the outer rotor type. However, contrary to these expectations, it was discovered that the electrical loading surface of the outer rotor type surpassed that of the inner

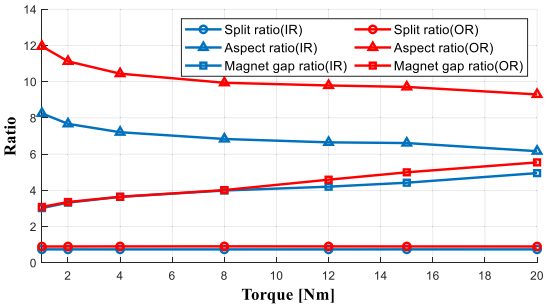

FIGURE 8. Key design parameters for both inner and outer rotor types across different torque levels based on the optimization results.

TABLE 8. Breakdown of the iron, pm, and coil weights.

Torque [Nm]	Inner rotor type			Outer rotor type		
	ϖ_{iron} [g]	ϖ_{PM} [g]	ϖ_{cu} [g]	ϖ_{iron} [g]	ϖ_{PM} [g]	ϖ_{cu} [g]
1	156.0	38.8	203.6	154.0	34.0	180.6
2	254.7	59.00	332.8	252.3	51.5	297.5
4	417.1	89.7	546.8	414.0	77.7	492.1
8	685.3	136.6	907.8	683.0	119.8	813.8
12	917.4	174.6	1210.5	932.0	170.9	1074.9
15	1083.6	205.1	1415.1	1109.4	209.6	1250.0
20	1327.8	273.00	1691.0	1393.0	274.5	1514.3

rotor type. Consequently, the outer rotor type enjoys a torque production advantage due to the larger values of both parameters (D and ξ_e) compared to those of the inner rotor type rather than the task of determining which parameter holds a more pronounced influence.

Fig. 8 displays the key design parameters for both the inner and outer rotor types across different torque levels, denoted as IR and OR, respectively. For the inner rotor type, achieving minimal active weight involves configuring the split ratio at approximately 0.74, while for the outer rotor type, a split ratio of around 0.90 is preferred to achieve the same outcome.

As the torque level increases, both the inner and outer rotor types exhibit a decline in aspect ratio coupled with an elevation in the magnet gap ratio. Notably, the aspect and magnet gap ratios are consistently greater for the outer rotor type than the inner rotor type. To generate equivalent torque, the inner rotor type necessitates an elongation in active length due to its smaller air gap diameter and electrical loading surface relative to the outer rotor type. Consequently, the aspect ratio of the inner rotor type remains smaller than its outer rotor counterpart.

Fig. 9 illustrates the torque performance comparison between the inner and outer rotor types. As evident from Fig. 9, the outer rotor type distinctly holds an edge over the inner rotor type in all factors, including weight, loss, and cost.

Table 8 presents a breakdown of the iron, permanent magnet, and coil weights within the inner and outer rotor types. Fig. 10 further illustrates the differences in weight for iron, permanent magnet, and coil components between these two rotor types. As shown in Fig. 10, the weight differences between the inner and outer rotor types of iron

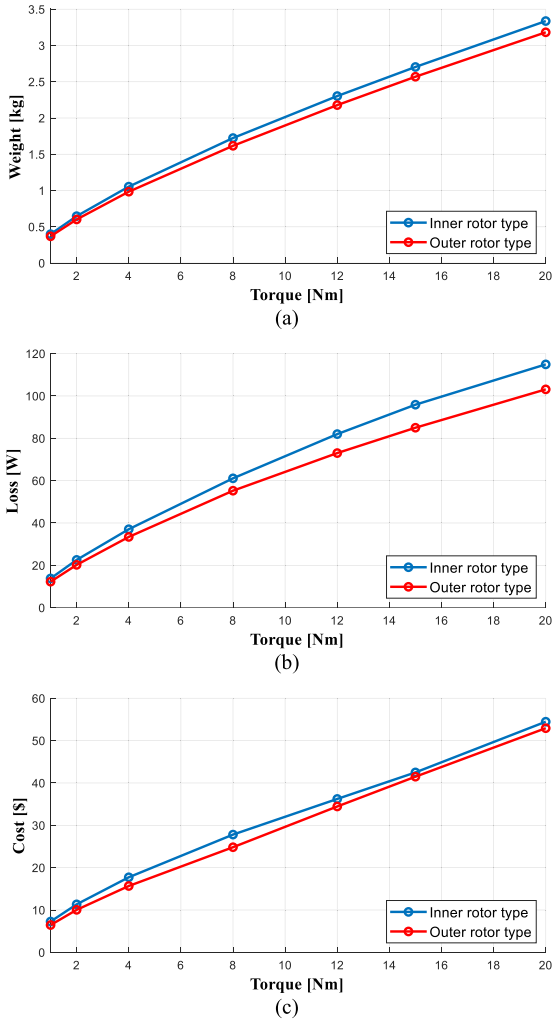

FIGURE 9. Performance comparison of inner and outer rotor types with respect to the torque. (a) weight, (b) loss, and (c) cost.

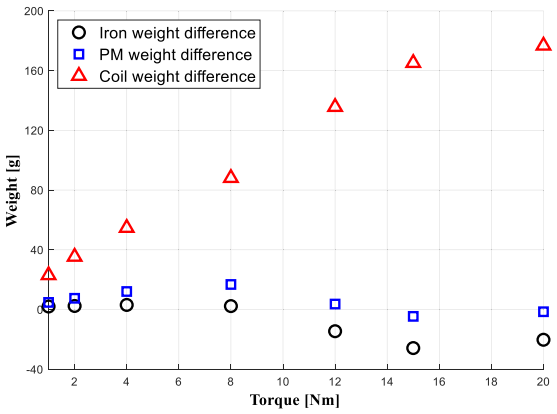

FIGURE 10. Weight differences for iron, PM, and coil components.

and permanent magnets do not hold substantial significance. Instances occur where the inner rotor type exhibits greater iron and permanent magnet weights than its outer rotor counterpart and vice versa. A notable contrast, however, emerges in terms of the coil weight. Specifically, the coil

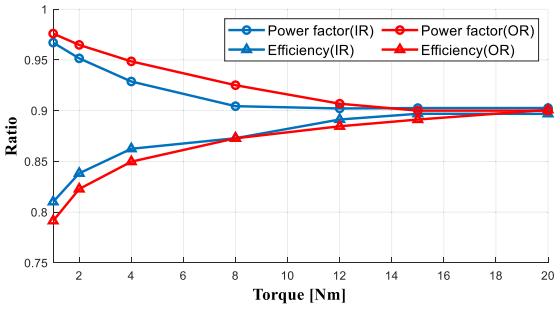

FIGURE 11. Power factor, and efficiency of inner and outer rotor types with respect to the torque.

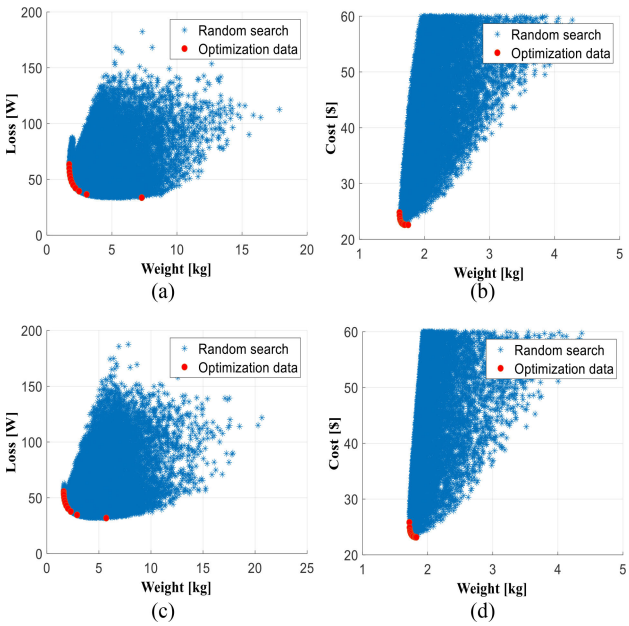

FIGURE 12. 2-D Pareto fronts: (a) weight-loss for inner rotor, (b) weight-cost for inner rotor, (c) weight-loss for outer rotor, and (d) weight-cost for outer.

weight significantly diverges between the inner and outer rotor types. This discrepancy shows the pivotal role of the coil in determining the active weight difference between the two rotor configurations. Furthermore, as mentioned in Section II, it is worth noting that the weight of the coil directly impacts copper loss. The relatively lower coil weight in the outer rotor type translates to reduced losses compared to the inner rotor type.

Fig. 11 displays the trends of power factor and efficiency across different torque levels for the inner and outer rotor types. As shown in Fig. 11, the power factor decreases, and efficiency increases as torque increases. In the low torque domain, the power factor of the inner rotor type is superior to that of the outer rotor type. On the other hand, in terms of efficiency, the outer rotor type is outstanding compared to the inner rotor type. The power factor and efficiency discrepancies between the inner and outer rotor types are negligible under high torque conditions.

Fig. 12 shows 2-D Pareto fronts illustrating weight-loss and weight-cost attributes for inner and outer rotor types. This

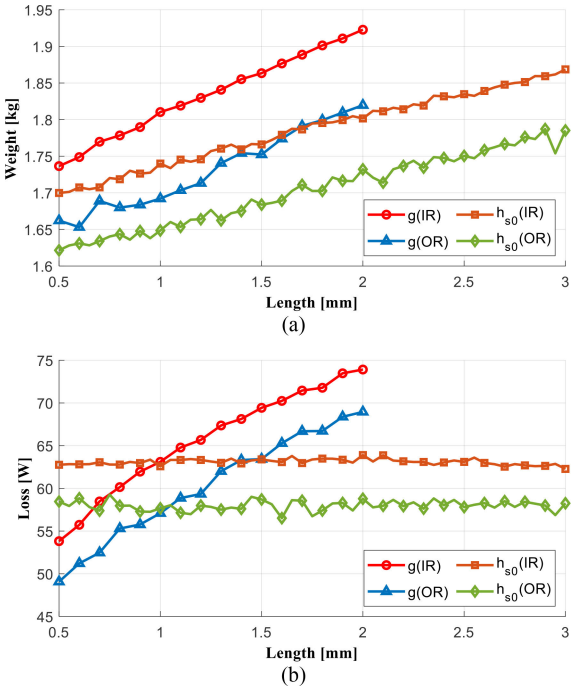

FIGURE 13. Performance trends of inner and outer rotor types with respect to air gap and slot opening weight.

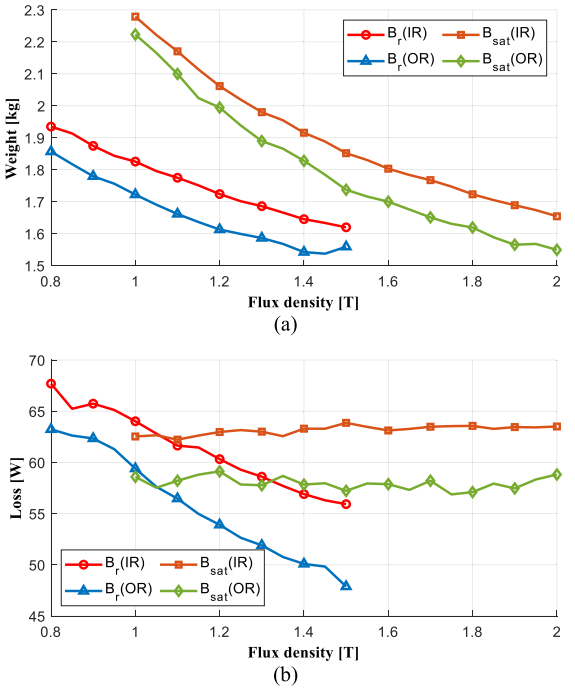

FIGURE 15. Performance trends of inner and outer rotor types with respect to residual flux density and saturation flux density.

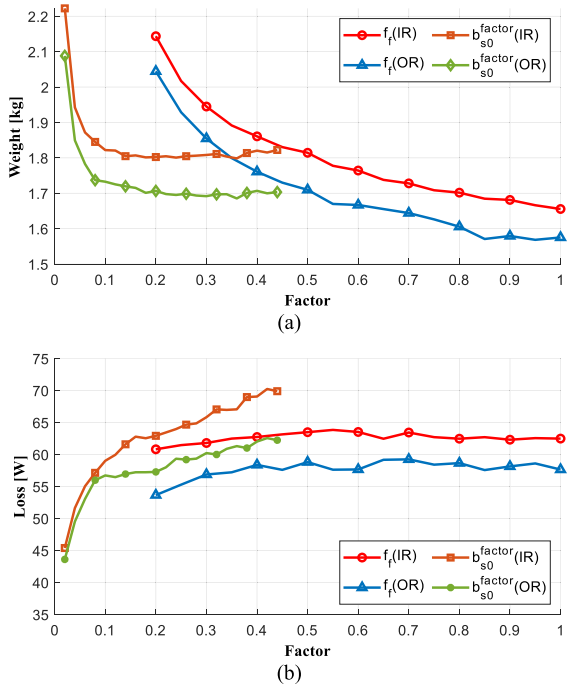

FIGURE 14. Performance trends of inner and outer rotor types with respect to fill factor and slot opening factor.

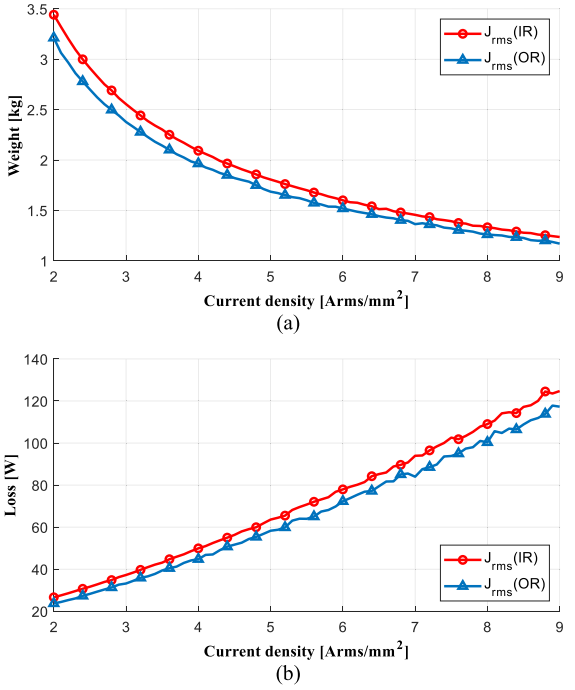

FIGURE 16. Performance trends of inner and outer rotor types with respect to current density.

depiction incorporates a collection of 50,000 randomized design candidates, all derived with a torque of 8 Nm. The visual representation in Fig. 12 demonstrates the validity and reliability of the optimization results.

Figs. 13-16 show the influence of parameter adjustments on motor performances. These figures illustrate the parameter variations carried out within the predefined ranges as outlined in Table 9 at a torque of 8 Nm. By a closer examination of Figs. 13-16, it becomes evident how these

TABLE 9. Predefined ranges of fixed parameters.

Parameter	Symbol	Unit	Range
Air gap	g	mm	[0.5, 2]
Fill factor	f_f	-	[0.2, 1]
Current density	J_{rms}	A_{rms}/mm^2	[2, 9]
Residual flux density	B_r	T	[0.8, 1.5]
Saturation flux density	B_{sat}	T	[1, 2]
Slot opening height	h_{s0}	mm	[0.5, 3]
Slot opening factor	b_{s0}^{factor}	-	[0.02, 0.44]

parameter alterations exert an impact on motor performances. Furthermore, they offer a basis for a comparative analysis of performance disparities between the inner and outer rotor types. The tendencies in performance alterations due to parameter variations are notably consistent for both the inner and outer rotor types. While the majority of parameters exert an influence on performance, the fill factor, saturation flux density, and slot opening height seem to exhibit negligible impact on losses. It is noteworthy that a substantial reduction in the slot opening factor to below 0.1 corresponds with a marked decrease in losses. Simultaneously, this reduction triggers a significant increase in weight, thus presenting a trade-off.

It is important to mention that all the data presented in Figs. 8-16 is derived from optimization rather than randomization, addressing a recurring issue identified in past published works. These datasets will hold considerable significance as reference materials for electric machine designers, particularly when the requirement arises to conduct comparisons between the inner and outer rotor types.

One thing to note is that aspects related to torque pulsation, such as cogging torque, have been excluded from the comparative analysis in this study. This decision was made because optimization of cogging torque can be achieved simply by adjusting ratio variables such as pole arc ratio during detailed design, without the need for optimization at the conceptual design stage [24].

V. CONCLUSION

This paper has analyzed and compared the performance characteristics of inner and outer rotor SPM machines by utilizing optimal design solutions chosen from a pool of numerous candidates. The integrated analytical model has been developed to achieve accurate and efficient optimization, capable of simultaneously addressing both rotor types. Consequently, three notable contributions, which have been lacking in previous research, can be summarized as follows:

1) In Section II, it is demonstrated that separate flux density computations for inner and outer rotor types are unnecessary. This insight leads to the consolidation of two equations into a single framework, thereby reducing computational time for the analytical-based optimization across inner and outer rotor types. This contribution further holds considerable academic merit.

2) In Section IV, the primary factor behind the outer rotor type's superiority over the inner rotor type is revealed by an extensive collection of optimization data. This can be attributed to the relatively lighter coil weight in the outer rotor configuration.

3) In Section IV, the optimization dataset shows the trends in key design parameters for both inner and outer rotor types. These datasets offer significant value as reference materials for electric machine designers, especially when the need arises for comprehensive comparisons and evaluations between the two rotor types.

REFERENCES

[1] L. Huang, J. Ji, W. Zhao, H. Tang, T. Tao, and S. Jin, "Direct torque control for dual three-phase permanent magnet motor with improved torque and flux," *IEEE Trans. Energy Convers.*, vol. 37, no. 4, pp. 2385–2397, Dec. 2022.

[2] S. G. Min, "Inductance calculation of coreless-type linear PM machines based on analytical field projection and coil separation method," *IEEE Trans. Magn.*, vol. 56, no. 9, Sep. 2020, Art. no. 8101511.

[3] D. K. K. Padinharu, G. J. Li, Z. Q. Zhu, R. Clark, A. Thomas, and Z. Azar, "AC losses in form-wound coils of surface mounted permanent magnet Vernier machines," *IEEE Trans. Magn.*, vol. 58, no. 6, Jun. 2022, Art. no. 8105315.

[4] G. K. Sakkas and A. G. Kladas, "Particular model for efficient switching frequency loss consideration in surface mounted permanent magnets," *IEEE Trans. Magn.*, vol. 59, no. 5, May 2023, Art. no. 7000505.

[5] Y. Zhao, Y. Li, and Q. Lu, "An accurate no-load analytical model of flat linear permanent magnet synchronous machine accounting for end effects," *IEEE Trans. Magn.*, vol. 59, no. 1, Jan. 2023, Art. no. 8100111.

[6] S. G. Min, "Modeling, investigation, and minimization of AC winding loss in slotless PM machines," *IEEE Trans. Energy Convers.*, vol. 36, no. 3, pp. 2249–2260, Sep. 2021.

[7] N. Verbeek and B. Dehez, "Comparison of inner and outer rotor configurations in slotless PM machines with PCB windings," in *Proc. IEEE Int. Electric Mach. Drives Conf. (IEMDC)*, May 2019, pp. 1–7.

[8] W. Chlebosz, G. Ombach, and J. Junak, "Comparison of permanent magnet brushless motor with outer and inner rotor used in e-bike," in *Proc. XIX Int. Conf. Electr. Mach. (ICEM)*, Rome, Italy, Sep. 2010, pp. 1–5.

[9] Y. Tani, S. Morimoto, and M. Sanada, "Influence of number of poles, magnet arrangement, and current density on characteristics of inner and outer rotor PMSMs," in *Proc. IEEE 9th Int. Conf. Power Electron. Drive Syst.*, Dec. 2011, pp. 711–716.

[10] M. Y. Arafat, M. Murshed, M. M. Hasan, and M. A. Razzak, "Design aspects and performance analysis of inner and outer rotor permanent magnet alternator for direct driven low-speed wind turbine," in *Proc. 2nd Int. Conf. Adv. Electr., Electron., Inf., Commun. Bio-Inform. (AEEICB)*, Feb. 2016, pp. 604–609.

[11] W. Q. Chu and Z. Q. Zhu, "Optimal split ratio and torque comparison of surface-mounted permanent magnet machines having inner or outer rotor," in *Proc. 6th IET Int. Conf. Power Electron., Mach. Drives (PEMD)*, Mar. 2012, pp. 1–6.

[12] M. Aydin, S. Huang, and T. A. Lipo, "Torque quality and comparison of internal and external rotor axial flux surface-magnet disc machines," *IEEE Trans. Ind. Electron.*, vol. 53, no. 3, pp. 822–830, Jun. 2006.

[13] L. J. Wu, Z. Q. Zhu, Y. T. Fang, and X. Y. Huang, "Difference in unbalanced magnetic force of fractional-slot PM machines between interna and external rotor topologies," *CES Trans. Electr. Mach. Syst.*, vol. 1, no. 2, pp. 154–163, Jul. 2017.

[14] A. Tovar-Barranco, A. López-de-Heredia, I. Villar, and F. Briz, "Modeling of end-space convection heat-transfer for internal and external rotor PMSMs with fractional-slot concentrated windings," *IEEE Trans. Ind. Electron.*, vol. 68, no. 3, pp. 1928–1937, Mar. 2021.

[15] W. Deng, S. Zuo, W. Chen, Z. Qian, C. Qian, and W. Cao, "Comparison of eccentricity impact on electromagnetic forces in internal- and external-rotor permanent magnet synchronous motors," *IEEE Trans. Transport. Electrific.*, vol. 8, no. 1, pp. 1242–1254, Mar. 2022.
[16] Y. Shi and T. W. Ching, "Power factor analysis of dual-stator permanent magnet Vernier motor with consideration on turn-number assignment of inner and outer stator windings," *IEEE Trans. Magn.*, vol. 57, no. 2, Feb. 2021, Art. no. 8200405.
[17] S.-W. Jung, J. Yoon, K. Choi, J. Bang, U. Bong, and S. Hahn, "Comparative design study of HTS synchronous motor with inner and outer rotor type based on multi-objective optimization," *IEEE Trans. Appl. Supercond.*, vol. 32, no. 6, Sep. 2022, Art. no. 5202305.
[18] D. Zarko, D. Ban, and T. A. Lipo, "Analytical calculation of magnetic field distribution in the slotted air gap of a surface permanent-magnet motor using complex relative air-gap permeance," *IEEE Trans. Magn.*, vol. 42, no. 7, pp. 1828–1837, Jul. 2006.
[19] W. Q. Chu, Z. Q. Zhu, and J. T. Chen, "Simplified analytical optimization and comparison of torque densities between electrically excited and permanent-magnet machines," *IEEE Trans. Ind. Electron.*, vol. 61, no. 9, pp. 5000–5011, Sep. 2014.
[20] D. H. Min and S. G. Min, "Optimal split ratio for high torque density PM machines based on analytical determination," *IEEE Trans. Transport. Electrific.*, early access, Jan. 2024, doi: 10.1109/TTE.2024.3356517.
[21] Z. Q. Zhu, D. Howe, and C. C. Chan, "Improved analytical model for predicting the magnetic field distribution in brushless permanent-magnet machines," *IEEE Trans. Magn.*, vol. 38, no. 1, pp. 229–238, Jan. 2002.
[22] S. G. Min and B. Sarlioglu, "Fast and systematic design optimization of surface-mounted PM machines using advanced analytical models and subharmonic elimination methods," *IEEE Trans. Magn.*, vol. 55, no. 1, Jan. 2019, Art. no. 8100216.
[23] R. Storn and K. Price, "Differential evolution a simple and efficient heuristic for global optimization over continuous spaces," *J. Global Optim.*, vol. 11, no. 4, pp. 341–359, 1997.
[24] S. G. Min, "Investigation of key parameters on cogging torque in permanent magnet machines based on dominant harmonic contents," *IEEE Trans. Transport. Electrific.*, vol. 10, no. 1, pp. 174–186, Mar. 2024.

DONG MYEONG CHOI (Student Member, IEEE) received the B.S. degree in electrical engineering from the Electric Machines and Optimization Data Analysis Laboratory (EMODAL), Soongsil University, Seoul, South Korea, in 2024.

His research interest includes analysis, design, modeling, and optimization of electric machines.

SEUN GUY MIN (Member, IEEE) received the B.S. degree in electrical engineering from Iowa State University, Ames, IA, USA, in 2010, and the M.S. and Ph.D. degrees in electrical engineering from the Wisconsin Electric Machines and Power Electronics Consortium (WEMPEC), University of Wisconsin, Madison, WI, USA, in 2013 and 2019, respectively.

From 2013 to 2016, he was the General Manager of electrical machines. From 2013 to 2016, he worked in the industry as the General Manager of the Electrical Machine Division of Research and Development, JUSTEK, Gyeonggi-do, South Korea. Since 2019, he has been an Assistant Professor with Soongsil University, Seoul, South Korea. During the Ph.D. program, he authored ten IEEE journal papers as the primary contributor, marking the highest number of first-author IEEE transaction papers published by any individual affiliated with WEMPEC since its inception, in 1981, with over 700 graduate students. His research interests include analysis, design, modeling, and optimization of electric machines, integrated electro-mechanical solutions for linear motion devices, predictive analytics and forecasting using machine/deep learning, and optimization data analysis based on robust evolutionary algorithms.